distribution of the source under consideration. A discussion of this question is to be found in § 4.11 of the IRAC Instrument Handbook[1] (version 1.0, 2010).

We have, in the face of these uncertainties, chosen to leave the flux ratio mapping and profiles unchanged. The maximum correction factors for the ratios are likely to be > 0.74, but less than unity, and ignoring this correction has little effect upon our interpretation of the results.

We have, finally, provided photometry for all of these sources, where the values were estimated by integrating within circular or polygonal apertures centred upon the nebulae; estimating the levels of background at various regions about the nebulae; applying the instrumental scattering corrections described above; and determined magnitudes using the α Lyrae calibration of Reach et al. (2006). The results are presented in Table 1.

3. DISCUSSION OF INDIVIDUAL PNE DETECTED IN THE GLIMPSE 3D SURVEY

We have obtained mapping and profiles for 14 PNe detected in the GLIMPSE 3D survey, and we shall present details of these sources in our analysis below. Images of six of the regions are also plotted in Figure 1, where we have combined 3.6 μm (blue), 4.5 μm (green) and 8.0 μm (red) IRAC imaging of the sources. It will be seen that most of the nebulae are relatively compact and ill-defined, although we see evidence for ring-like structures in IC 4674, H 1-6 and M 1-29, and for bipolarity in G009.8-01.1 (otherwise known as PHR1811-2100).

Although the range of bright high S/N sources is therefore less extensive than for GLIMPSE I & II (see e.g., Phillips & Ramos-Larios 2008a; Ramos-Larios & Phillips 2008), we are able to draw interesting conclusions concerning the properties of these nebulae.

3.1. *Pe 2–12*

This is a relatively little studied PN which appears to have an elliptical morphology (Figure 1), and an optical diameter of ∼5 arcsec (Cahn & Kaler 1971). Shell densities appear to be of order 1.1×10^3 cm^{-3} (although this value has a large range of uncertainty; see Chiappini et al. 2009), whilst the He/H abundance ratio is $\cong 0.072$, and N/O $\cong 0.714$ (Chiappini et al. 2009).

It is apparent that whilst the optical dimensions are comparable to those at 3.6 and 4.5 μm (see Figure 2), they are significantly less than those observed at larger MIR wavelengths. Such trends are partly affected by the differing instrumental sensitivities in the various IRAC channels, the values of contour level cut-off, and variation of source flux with wavelength, all of which may influence the apparent size of the envelope.

There is nevertheless clear evidence that this increase in size reflects a real trend in source dimensions. Logarithmic profiles through the centre of the source permit integration over several pixels, for instance, and lead to higher levels of S/N. These also show an increase in width with increasing IRAC wavelength. Where one ignores the trends observed at 3.6 μm (background field star contamination is extremely high in this channel), then we

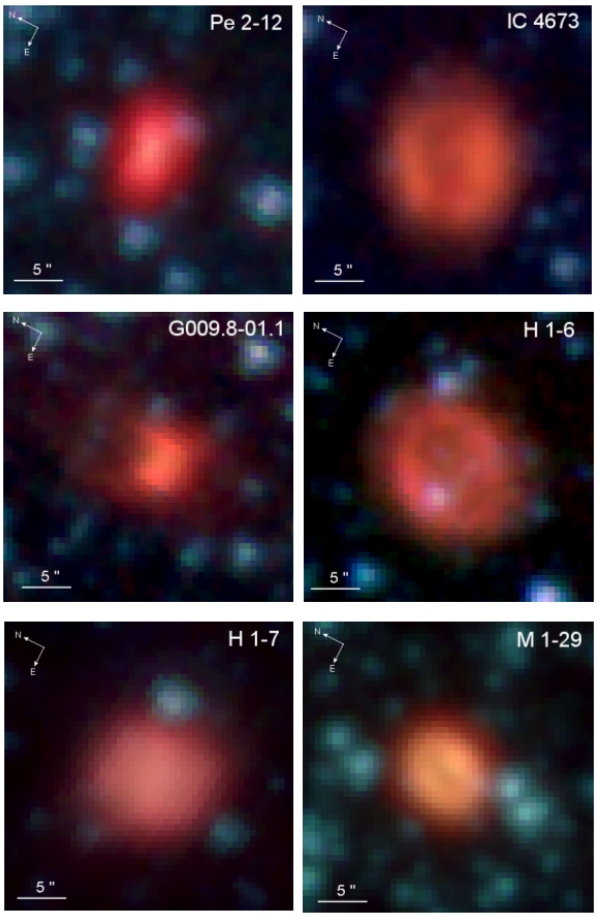

Fig. 1. Images of six planetary nebulae observed during the *Spitzer* GLIMPSE 3D survey, where 3.6 μm emission is represented as blue, 4.5 μm emission as green, and 8.0 μm emission as red. Three of the sources appear to have internal ring-like structures (viz. IC 4673, H 1-6 and M 1-29), whilst the MASH I source G009.8-01.1 (PHR1811-2100) has a bipolar morphology. The color figure can be viewed online.

[1] http://ssc.spitzer.caltech.edu/irac/iracinstrumenthandbook/IRAC_Instrument_Handbook.pdf.